Origin of weak layer contraction in de Vries smectic liquid crystals

Dena M. Agra-Kooijman,[1] HyungGuen Yoon,[2] Sonal Dey,[1] and Satyendra Kumar[1,*]
[1]*Department of Physics, Kent State University, Kent, Ohio 44242, USA*
[2]*TV Development Team, LCD Business, Samsung Display, Chungcheongnam-Do 336-741, Korea*
(Received 17 July 2013; revised manuscript received 27 November 2013; published 21 March 2014)

Structural investigations of the de Vries smectic-*A* (Sm*A*) and smectic-*C* (Sm*C*) phases of four mesogens containing a trisiloxane end segment reveal a linear molecular conformation in the Sm*A* phase and a bent conformation resembling a hockey stick in the Sm*C* phase. The siloxane and the hydrocarbon parts of the molecule tilt at different angles relative to the smectic layer normal and are oriented along different directions. For the compounds investigated, the shape of orientational distribution function (ODF) is found to be *sugarloaf* shaped and not the widely expected *volcano like* with positive orientational order parameters: $\langle P_2\rangle = 0.53$–$0.78$, $\langle P_4\rangle = 0.14$–$0.45$, and $\langle P_6\rangle \sim 0.10$. The increase in the effective molecular length, and consequently in the smectic layer spacing caused by reduced fluctuations and the corresponding narrowing of the ODF, counteracts the effect of molecular tilt and significantly reduces the Sm*C* layer contraction. Maximum tilt of the hydrocarbon part of the molecule lies between approximately 18° and 25° and between 6° and 12° for the siloxane part. The critical exponent of the tilt order parameter, $\beta \sim 0.25$, is in agreement with tricritical behavior at the Sm*A*–Sm*C* transition for two compounds and has lower value for first-order transition in the other compounds with finite enthalpy of transition.

DOI: 10.1103/PhysRevE.89.032506 PACS number(s): 61.30.Gd, 61.30.Eb, 64.70.mj

Thermotropic smectic liquid crystal (LC) phases are layer structures characterized [1] by a mass density wave in one direction, specified by a unit vector $\boldsymbol{k}$. In the smectic-*A* (Sm*A*) phase, the director $\boldsymbol{n}$ (i.e., the direction of alignment of calamitic mesogens) is parallel to $\boldsymbol{k}$. But, $\boldsymbol{n}$ is tilted with respect to $\boldsymbol{k}$ at a temperature-dependent angle α in the smectic-*C* (Sm*C*) phase. In *conventional* smectic materials, α varies from zero to ∼30° causing the layers to shrink by $\cos\alpha$, which may be [2–4] as high as 13%. The shrinkage induces chevron defects [5] that manifest in zigzag defects in ferroelectric Sm-*C* electro-optical devices. They are the major impediment to the commercialization of ferroelectric smectic devices that switch ∼1000 times faster and have higher contrast [6] than the ubiquitous nematic LC devices.

In 1979, de Vries reported [7,8] a different kind of Sm*C* phase having ten times smaller (∼1%) layer shrinkage than the conventional Sm*C* phase [9,10]. Since then, a large number of mesogens incorporating a fluorinated or siloxanated segment have been reported to form the so-called *de Vries smectic* phases. These materials provide a pathway to ferroelectric devices [5,6] free from zigzag defects. To explain the absence of large layer contraction, de Vries proposed the *diffuse-cone* model [7,8,11] which assumes that local directors in the Sm*A* phase are tilted at a large polar angle but have *overall* azimuthal degeneracy. Upon transition to the Sm*C* phase, the azimuthal degeneracy is lost as the molecular distribution gradually gravitates towards a preferred azimuthal angle with almost no change in the polar tilt and minimal layer shrinkage. In an alternative model [12–14], the de Vries phases are expected to be similar to the conventional smectics but with low orientational order and highly condensed smectic density wave.

The two models differ in the molecular orientational distribution function (ODF), $f(\theta)$, where θ is the angle between the long axis of an individual molecule and the director $\boldsymbol{n}$. In the first case, the shape of $f(\theta)$ in the Sm*A* phase is *volcano like* while in the second case, it is *sugarloaf like* having Gaussian probability density [12] with its maximum along $\boldsymbol{n} \| \boldsymbol{k}$. The function $f(\theta)$ is a sum of even Legendre polynomials $\langle P_n(\cos\theta)\rangle$, higher-order terms being of diminishing significance. The second term $\langle P_4\rangle$ should be negative (positive) for the volcano- (sugarloaf-) shaped [12,15] distribution. Theoretical models [16–19] predict the nature of the Sm*A* to Sm*C* (*AC*) transition in de Vries smectics to be near a tricritical point [20,21]. The first-order *AC* transition [22,23] was reported to originate from a disorder condensation mechanism [24]. Phenomenological molecular-statistical theory [18,15] uses a complete set of orientational order parameters to explain the weak layer contraction while Osipov [15] has suggested that the tilt-induced contraction is *somehow* significantly compensated. The origin of the compensation has remained a mystery.

In a recent paper [20], direct x-ray measurements of the orientational order parameters of the hydrocarbon and siloxane parts of the mesogens, and the director tilt in the Sm*C* phase, were reported. The results were significantly different from previously reported measurements. For example, the order parameter S and molecular tilt $\alpha(T)$ were larger and the latter was close to the value expected from optical measurements on other compounds. While these results were fully consistent with the de Vries diffuse-cone model, they did not expressly confirm it. No evidence to validate either of the two possible ODFs was presented in [20] or any other previous publications. The experimental results reported in this paper provide a more complete picture of these phases with several surprising findings. The results specifically reveal that (i) the shape of the ODF is *sugarloaf* in the Sm*A* and Sm*C* phases, (ii) the siloxane (Si) segments are orientationally ordered and collinear with the molecules in the Sm*A* phase, (iii) siloxane segments tilt at a smaller angle with respect to $\boldsymbol{k}$ than the remainder hydrocarbon

*Corresponding author: skumar@kent.edu

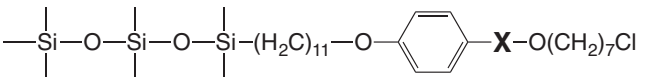

Label	X	Transition Temperatures
A		Cr ←26°C— SmC ←84°C— SmA ←98°C— I
B		Cr ←44°C— SmC ←78°C— SmA ←90°C— I

FIG. 1. Molecular structures of compounds ***A*** and ***B***, their phase sequence, and transition temperatures.

(HC) part of the molecule in the Sm*C* phase causing it to resemble a hockey stick, (iv) orientational ordering of siloxane segments is weaker than of the HC part of the molecule in both phases, (v) siloxane segments in end chains tend to nanosegregate [25–28] and enhance smectic order [29], and (vi) most importantly, the tilt-induced layer shrinkage is compensated by decreasing molecular fluctuations and narrowing of the ODF in the Sm*C* phase.

We report results of synchrotron x-ray investigations of the two compounds, ***A*** and ***B***, shown in Fig. 1. Results on two other compounds, previously referred to as ***C*4** and ***C*9**, in Ref. [20], were further analyzed and are included in this paper for a more complete picture. The x-ray experiments were performed using 16.2 keV ($\lambda = 0.76534$ Å) radiation and 200 μm × 200 μm beam cross section at the undulator station 6IDB of the Advanced Photon Source. The x-ray beam was sufficiently attenuated to avoid radiation damage to samples. Samples were flame sealed in 1.5-mm quartz capillaries and placed inside a hot stage (Instec HCS402). An image plate detector MAR345 was placed at 498.42 mm from the sample to cover a wide q range. Well-aligned samples were obtained by repeated heating and slow cooling across the clearing point. Data were analyzed after calibrating against silicon standard (NIST 640C) and subtracting the background measured with an empty capillary. Radial (I vs q) and azimuthal (or χ-) scans were generated from diffraction patterns using the software package FIT2D [30].

Representative x-ray patterns in the Sm*A* and Sm*C* phases of ***B*** are shown in Fig. 2. Temperature dependence of smectic layer spacing, d, calculated from the first small-angle peak reveals a 1.2% and 1.1% layer shrinkage in the Sm-*C* phase of ***A*** and ***B***, respectively. Presence of the second and third multiples of the primary peak confirms a highly condensed smectic density wave attributed to nanosegregation [31,32] induced by the siloxane segments. The magnitude of the smectic order parameter, $|\Psi|$, was estimated using the Leadbetter method [11,33] and found to be ∼0.74 ± 0.02 in the Sm*C* phase of both compounds.

The two wide-angle diffuse arcs indicated by red arrows in Fig. 2 arise from average lateral separation between well-aligned Si segments (∼6.8 Å) and HC (∼4.5 Å) parts of the molecules. The separation of Si and HC peaks further confirms their nanosegregation. Azimuthal intensity distribution of

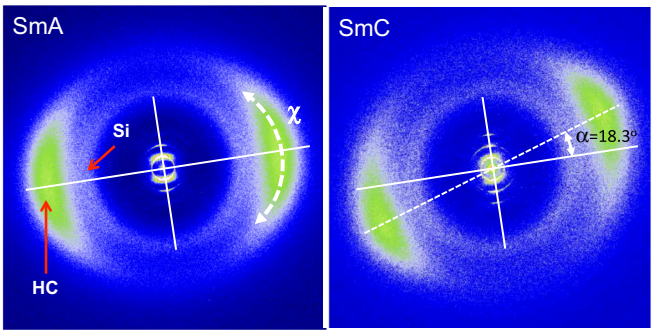

FIG. 2. (Color online) X-ray diffraction patterns in the Sm*A* (86.5 °C) and the Sm*C* (51.7 °C) phases of ***B*** reveal the hydrocarbon (HC, green) and siloxane (Si, white) peaks. The dashed line drawn on the Sm*C* pattern shows a shift of 18.3° caused by director tilt from its position (solid line) in the Sm*A* phase.

these peaks depends on the orientational order of the two parts of the molecule. The angular separation between the peaks of the large-angle (red square and green circle) and small-angle (blue triangle) peaks in their χ scans, Fig. 3, is a direct measure of the tilt angle α. It is evident that both the Si and the HC peaks are collinear and perpendicular to the direction of the small-angle peaks in the Sm*A* phase; see Figs. 2 and 3(a). At 51.7 °C (i.e., $T - T_{AC} = -26.3$ °C) in the Sm*C* phase, the HC part is tilted at ∼18.3° as indicated in Figs. 2 and 3(b) while the Si segments are tilted at a much smaller angle of ∼4.6° giving the molecules a hockey-stick shape; see inset in Fig. 4(c). This is *direct evidence* of hockey-stick like molecular conformation in the Sm*C* phase with a temperature-dependent kink at the point where the Si segment meets the HC part. The angle of kink is $\Delta\chi = 18.3° - 4.6° \cong 13.7°$ for compounds ***A*** and ***B*** at 30 °C below T_{AC}, and ∼9.3° for compound ***C*4** at 20 °C below T_{AC}, as shown in Fig. 4(c). Although various theoretical models envisage [15,34,35] bent molecular conformations, those are of very different nature and involve bending of terminal chains with respect to the rigid central core of the molecule. Single power law fits to the measured HC tilt angle yield the critical exponent $\beta = 0.25 \pm 0.03$ and $\beta = 0.26 \pm 0.01$ for compound ***A*** and ***C*4** [20], respectively, and 0.21 ± 0.02 for ***B*** and ***C*9**. Here, T_c is the second-order *AC* transition temperature. These values of β for compound ***A*** and ***C*4** are consistent with the predicted tricritical behavior. Its somewhat smaller value for ***B*** and ***C*9** is indicative of weakly first-order nature of this transition with nonzero value of the enthalpy change $\Delta H_{AC} = 0.16$ kJ/mol [36] for compound ***B*** and 1.7 kJ/mol for ***C*9** [20].

The functions $f(\theta)$ are determined from χ scans of the HC peaks at representative temperatures in the Sm*A* and Sm*C* phases by numerical inversion using the method of Davidson *et al.* [37], and are shown in Fig. 5 for the four compounds. The orientational order parameters $\langle P_2\rangle = \frac{1}{2}\,[3\langle\cos^2\theta\rangle - 1]$, $\langle P_4\rangle = 1/8\,[3 - 30\langle\cos^2\theta\rangle + 35\langle\cos^4\theta\rangle]$, and $\langle P_6\rangle = 1/16\,[-5 + 105\langle\cos^2\theta\rangle - 315\langle\cos^4\theta\rangle + 231\langle\cos^6\theta\rangle]$ are then calculated by substituting them for "X" in Eq. (1):

$$\langle X\rangle = \frac{\int_0^{\pi/2} X f(\theta)\sin\theta d\theta}{\int_0^{\pi/2} f(\theta)\sin\theta d\theta}. \quad (1)$$

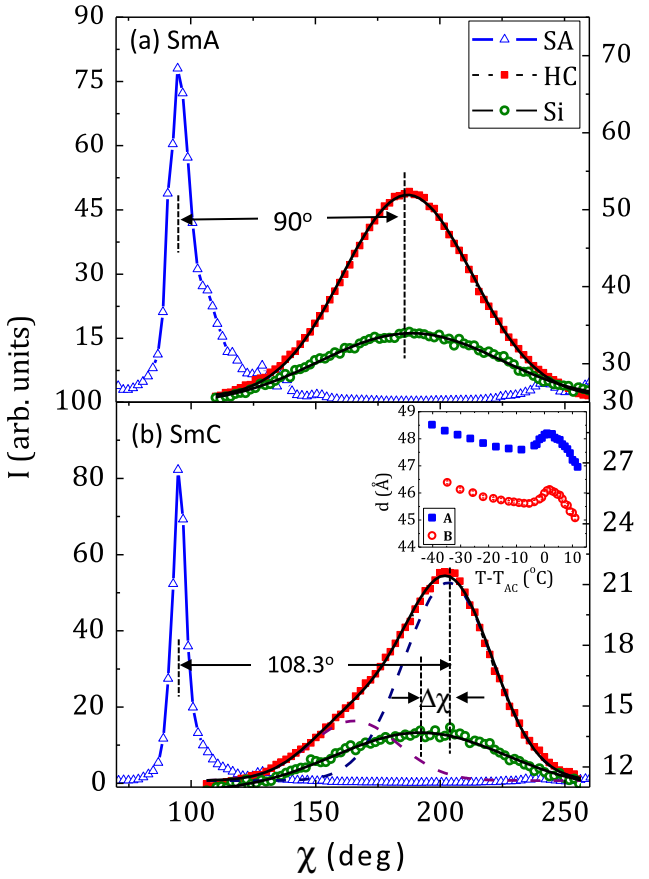

FIG. 3. (Color online) Azimuthal peak profiles of the small-angle (SA) (blue triangles, left ordinate axis), and wide-angle peaks (right ordinate axis): HC (red squares), and Si (green circles) for compound ***B*** in the Sm*A* (86.5 °C) and Sm*C* (51.7 °C) phases. The difference between the tilts of HC and Si segment, $\Delta\chi = 13.7°$ in (b). The black solid lines through the HC and Si peaks are fits. In (b), the fit to HC peak is a composite of two Gaussians (dashed lines) to two domains. Inset in (b): Layer spacing for compounds **A** and **B**.

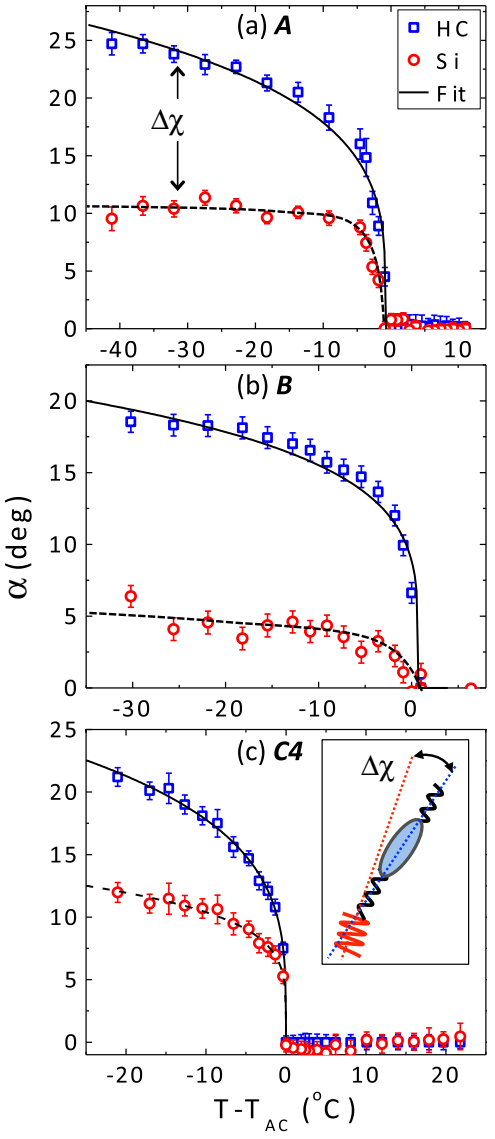

FIG. 4. (Color online) Temperature dependence of the tilt angles of hydrocarbon (blue squares) and siloxane (red circles) segments for (a) ***A***, (b) ***B***, and (c) ***C*4**. The inset in (c) schematically shows the Si segment (red) and the HC (black) parts of the Sm*C* phase. Solid lines are fits to a single power law; dashed lines are drawn as guide to the eye.

These parameters are plotted in Fig. 6 as functions of temperature. Values of the $\langle P_2\rangle$ for all compounds show similar temperature dependence but its values for compounds ***C*4** and ***C*9** are slightly higher than for ***A*** and ***B***. It should be noted that while $\langle P_4\rangle$ has previously been measured for a handful of de Vries compounds using the polarized Raman spectroscopy [14,32,38] and x-ray scattering methods [39], values of $\langle P_6\rangle$ have previously not been measured for any LC system. The values of the three parameters remain essentially constant in the Sm*A* phase. In the Sm*C* phase, $\langle P_2\rangle$ increases from ~0.52 to ~0.67 for ***A*** and from ~0.53 to ~0.64 for ***B*** before leveling off. These values are close to the values for compounds with fluorinated end segment [40] but somewhat higher than other organosiloxane mesogens [25–28]. The value of $\langle P_2\rangle$ for the Si segments remains essentially constant at ~0.40 in both phases of all four compounds, and is not plotted.

The values of $\langle P_4\rangle$ are constant at $+0.14 \pm 0.01$ in the Sm*A* phase for compounds ***A*** and ***B*** and then increase to $+0.36 \pm 0.01$ and $+0.30 \pm 0.01$ in their respective Sm*C* phase. The values of $\langle P_4\rangle$ for ***C*4**, which has the widest Sm*A* range, lie between 0.26 ± 0.02 and 0.38 ± 0.02, and show a slight decrease with temperature in the Sm*A* phase. Its value appears somewhat constant for the other three compounds. It is noteworthy that $\langle P_4\rangle$ remains positive (consistent with a sugarloaf ODF) and increases to 0.41 ± 0.02 and 0.3 ± 0.03 in Sm*C* phase for ***C*4** and ***C*9**, respectively. There has been only one report of a negative but small value of $\langle P_4\rangle$ (~–0.05) for the compound TSiKN65 [38]. However, its chemical structure is different from the four compounds investigated in this study and it forms a chiral ferroelectric smectic phase. The values of $\langle P_6\rangle$ are small in the Sm*A* phase and reach a value of $\sim 0.10 \pm 0.03$ in the Sm*C* phase of all compounds.

The positive values of $\langle P_4\rangle$ are consistent with the calculated sugarloaf like ODFs, shown in Fig. 5 for the Sm*A*

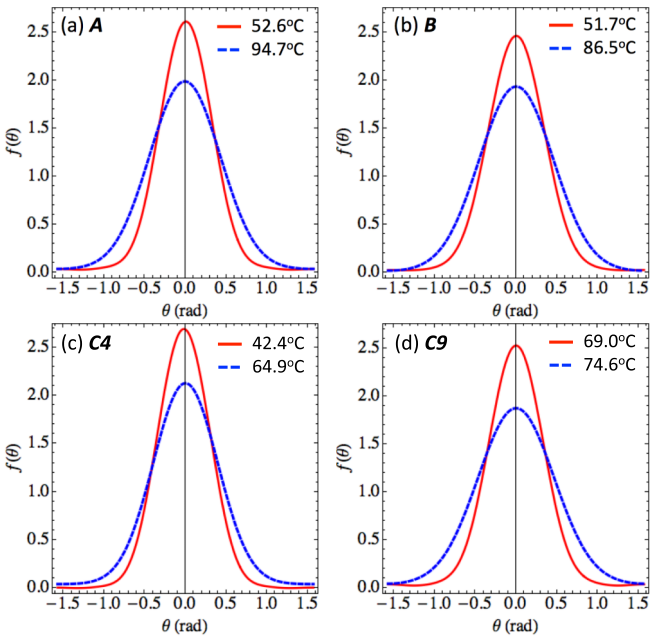

FIG. 5. (Color online) Sugarloaf like orientational distribution function in the SmA (dashed blue line) and SmC (solid red line) phases for compound (a) ***A*** and (b) ***B***, (c) ***C4***, and (d) ***C9***. The center of $f(\theta)$ in SmC phase is shifted to coincide with that of SmA.

and SmC phases. However, this result on nonchiral systems does not necessarily rule out the diffuse-cone model which has been successfully used to explain the unusually large, or *giant*, electroclinic effect [23,41,42] in the chiral SmA* phase of several compounds. The average orientational fluctuation about the director $\boldsymbol{n}$ can be estimated from $\langle\cos\theta\rangle\sim0.80$ which is calculated in the SmA phase of compound ***A***

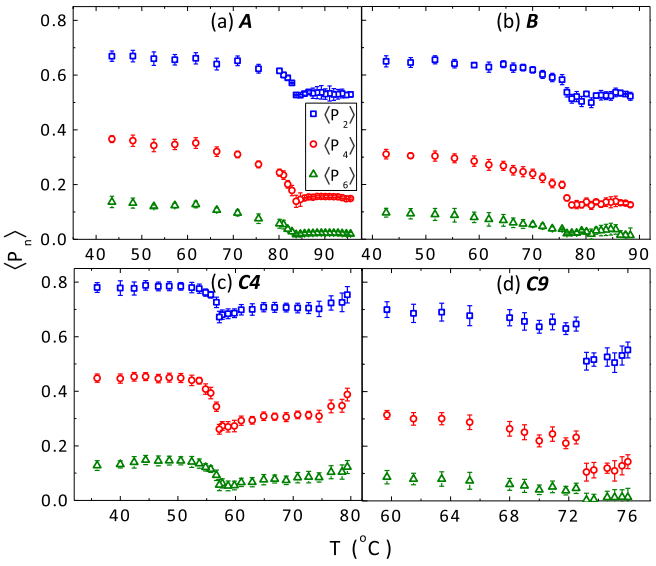

FIG. 6. (Color online) Temperature dependence of orientational parameters $\langle P_2\rangle$ (blue squares), $\langle P_4\rangle$ (red circles) and $\langle P_6\rangle$ (green triangles) for the hydrocarbon part of mesogens (a) ***A***, (b) ***B***, (c) ***C4***, and (d) ***C9***.

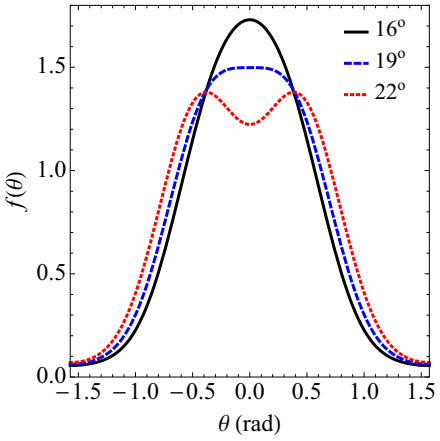

FIG. 7. (Color online) The simulated ODFs with respect to the SmA layer normal $\boldsymbol{k}$ for polar tilt angles of 16°, 19°, and 22° using an experimentally measured SmC ODF with corresponding molecular orientational fluctuations $\langle\theta\rangle = 19°$ about the director $\boldsymbol{n}$.

using Eq. (1) with $X = \cos\theta$. The corresponding average molecular fluctuation $\langle\theta\rangle$, also calculated from Eq. (1) at the same temperature, is approximately 33° which is much larger than the largest measured value of molecular polar tilt $\alpha\sim25°$ measured in the SmC phase. Clearly, molecular fluctuations larger than the molecular tilt will obscure any decrease in the ODF at its center making even the conical distribution of molecules to appear as sugarloaf. To illustrate this, intensity distribution from one of the ODFs in the SmC phase corresponding $\langle\theta\rangle\sim19°$ was used to simulate three ODFs in the SmA phase with respect to the direction $\boldsymbol{k}$ and for polar tilt (or, diffuse cone) angle α (=16°) smaller, (19°) equal, and (22°) larger than $\langle\theta\rangle$. Since one measures the molecular distribution in the plane perpendicular to the x-ray scattering vector, the calculations were done by convolving the two intensity distributions tilted at angles of $\pm\,\alpha$ relative to $\boldsymbol{k}$ in that plane. The ODF of the resultant distribution was then determined using the method of Davidson *et al*. The results, in Fig. 7, clearly show that it is difficult to directly measure a volcano like distribution unless α is larger than $\langle\theta\rangle$.

It should also be pointed out that there is no *a priori* reason to rule out the possibility of the ODF being volcano like in the SmA phase of chiral systems and sugarloaf like in the nonchiral SmA systems. In order to clearly demonstrate diffuse-cone ODF, one needs a system with smaller molecular fluctuations in the SmA phase, i.e., higher $\langle P_2\rangle$. We plan to investigate other chiral and nonchiral de Vries materials to test if any of them unambiguously reveals a volcano like ODF.

The ODFs of the four systems investigated are similar to those of conventional smectics but with a lower $\langle P_2\rangle$ and highly condensed smectic density wave. The width of $f(\theta)$ decreases with decreasing temperature and becomes much narrower in the SmC phase. The narrowing of $f(\theta)$ apparently increases the average effective molecular length thereby compensating the decrease in smectic layer spacing caused by increasing tilt in the SmC phase. We calculated the effective length L of the molecule from

$$d(T) = L\,\langle\cos\theta\rangle\cos\alpha(T). \qquad (2)$$

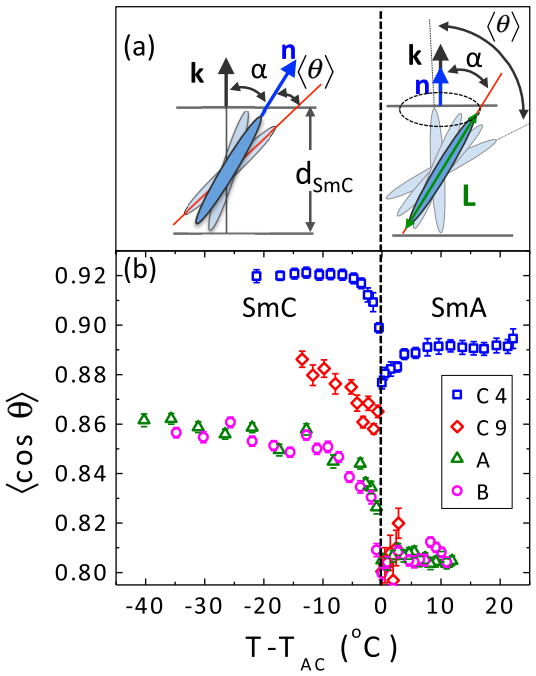

FIG. 8. (Color online) (a) Schematic of molecular orientation in the de Vries (right) SmA and (left) SmC phases. Molecules lie on the surface of a cone with polar tilt angle α and average molecular fluctuations of $\langle\theta\rangle$; (b) temperature dependences of $\langle\cos\theta\rangle$ for compounds $\boldsymbol{A}$, $\boldsymbol{B}$, $\boldsymbol{C4}$, and $\boldsymbol{C9}$.

where $d(T)$ and $\alpha(T)$ are measured experimentally. The term $\langle\cos\theta\rangle$ represents average molecular fluctuations [Fig. 8(a)] about $\boldsymbol{n}$ and is reflected in the width of the ODF. The value of $\langle\cos\theta\rangle \sim 0.80$ in the SmA phase increases to ~ 0.86 in the SmC phase of compounds $\boldsymbol{C4}$ and $\boldsymbol{C9}$. Its temperature dependence is shown in Fig. 8(b). This increase counteracts the layer shrinkage caused by the increasing tilt α, leading to a much reduced layer contraction. In the SmA phase, L increases linearly with temperature from ~ 58.5 to 60.0 Å for $\boldsymbol{A}$, and from ~ 56.0 to 58.0 Å for $\boldsymbol{B}$. Temperature dependence of L in the SmC phase has the same value, -0.040 ± 0.007 Å/deg C, for both compounds. This can be attributed to stiffening [2,3] of the molecule as in conventional LCs. Clearly the layer contraction in the SmC phase is significantly diminished by the increase in $\langle\cos\theta\rangle$.

Interestingly, both the hydrocarbon and siloxane parts of the molecule orient along the director $\boldsymbol{n}$ in the SmA phase but at different angles α_1 and α_2 in the SmC phase. Consequently, the molecules develop a kink in the SmC phase at the site where HC and Si parts meet. If we use $\boldsymbol{n}$ to specify the direction of one (the HC) part and $\boldsymbol{n'}$ for the other (Si) part, then $\boldsymbol{n}$ and $\boldsymbol{n'}$ are collinear (noncollinear) in the de Vries SmA (SmC) phase. In both phases, the degree of orientational order, S_1, of one (hydrocarbon) part is much larger than (S_2) that of the second (siloxane) part as previously reported [20]. In the SmC phase, the tilt angles α_1 and α_2 for $\boldsymbol{n}$ and $\boldsymbol{n'}$ with respect to the smectic layer normal $\boldsymbol{k}$ are needed to specify the phase completely. When these findings are considered with the need of two smectic order parameters, say Ψ_1 and Ψ_2, representing the conventional smectic density and the dipolar density waves to describe the *frustrated* smectic [43–46] phases, it becomes apparent that one needs pairs of the four parameters, namely $\boldsymbol{n}$ and $\boldsymbol{n'}$, S_1 and S_2, α_1 and α_2, and Ψ_1 and Ψ_2 to specify the relevant calamitic LC phases as outlined in Table I.

TABLE I. Liquid crystal phases and the associated order parameters. Here, the use of "$\parallel$" and "$\angle$" between unit vectors indicates that they are parallel and oblique to each other, respectively, while "—" stands for the corresponding parameters not being applicable. For brevity's sake, the in-plane SmC director is not included in this table.

	Parameters					
Phase	$\boldsymbol{n}, \boldsymbol{n'}, \mathbf{k}$	S_1	S_2	α_1 and α_2	Ψ_1	Ψ_2
Nematic	$\boldsymbol{n}\parallel\boldsymbol{n'}$	$\neq 0$	—	—	—	—
Biaxial nematic	$\boldsymbol{n}\angle\boldsymbol{n'}$	$\neq 0$	$\neq 0$	—	—	—
SmA and SmA_1	$\boldsymbol{n}\parallel\boldsymbol{n'}\parallel\mathbf{k}$	$\neq 0$	—	$\alpha_1 = \alpha_2 = 0$	$\neq 0$	0
SmC and SmC_1	$n\parallel n'\angle\mathrm{k}$	$\neq 0$	—	$\alpha_1 = \alpha_2 \neq 0$	$\neq 0$	0
de Vries SmA	$\boldsymbol{n}\parallel\boldsymbol{n'}\parallel\mathbf{k}$	$\neq 0$	$\neq 0$	$\alpha_1 = \alpha_2 = 0$	$\neq 0$	0
de Vries SmC	$\boldsymbol{n}\angle\boldsymbol{n'}\angle\mathbf{k}$	$\neq 0$	$\neq 0$	$\alpha_1 \neq \alpha_2 \neq 0$	$\neq 0$	0
SmA_2 and SmA_d	$\boldsymbol{n}\parallel\boldsymbol{n'}\parallel\mathbf{k}$	$\neq 0$	—	$\alpha_1 = \alpha_2 = 0$	$\neq 0$	$\neq 0$
SmC_2	$\boldsymbol{n}\parallel\boldsymbol{n'}\angle\mathbf{k}$	$\neq 0$	$\neq 0$	$\alpha_1 = \alpha_2 \neq 0$	$\neq 0$	$\neq 0$

To summarize, we have presented direct evidence for kinked molecular conformation in the SmC phase and determined order parameters $\langle P_2\rangle$, $\langle P_4\rangle$, and $\langle P_6\rangle$ in the SmA and SmC phases. The values of $\langle P_4\rangle$ are positive and consequently, the shape of the ODF is apparently sugarloaf like for both compounds. Furthermore, narrowing of the ODFs in the SmC phase significantly compensates for the layer shrinkage caused by the increasing director tilt, and is the *missing factor* responsible for rendering the layer contraction much smaller than in the conventional smectics. These results provide a major advancement in our understanding of the de Vries smectics.

The U.S. Department of Energy (DOE), Office of Science (OS), Basic Energy Sciences (BES) supported this work under Grant No. DE-SC-0001412. X-ray experiments were performed on beamline 6-ID-B of the X-ray Science Division at Sector 6 at the APS, Argonne National Laboratory. Use of the Advanced Photon Source (APS) was supported by the DOE, OS, BES under Contract No. DE-AC02-06CH11357. The authors thank Robert Lemieux for providing us the four compounds, and Noel Clark, Peter Collings, Frank Giesselmann, David Allender, and Jacques Prost for very useful discussions.

[1] P. G. de Gennes and J. Prost, *The Physics of Liquid Crystals* (Oxford University Press, New York, 1993), p. 18.

[2] S. Kumar, Phys. Rev. A **23**, 3207 (1981).

[3] C. R. Safinya, R. J. Birgeneau, J. D. Litster, and M. E. Neubert, Phys. Rev. Lett. **47**, 668 (1981).

[4] J. P. Lagerwall and F. Giesselmann, Chem. Phys. Chem. **7**, 20 (2006).
[5] T. P. Rieker, N. A. Clark, G. S. Smith, D. S. Parmar, E. B. Sirota, and C. R. Safinya, Phys. Rev. Lett. **59**, 2658 (1987).
[6] N. A. Clark and S. T. Lagerwall, Appl. Phys. Lett. **36**, 899 (1980).
[7] A. de Vries, A. Ekachai, and N. Spielberg, Mol. Cryst. Liq. Cryst. **49**, 143 (1979); J. Phys. (Paris) **40**, C3-147 (1979).
[8] A. de Vries, J. Chem. Phys. **71**, 25 (1979).
[9] J. Naciri, J. Ruth, G. Crawford, R. Shashidhar, and B. R. Ratna, Chem. Mater. **7**, 1397 (1995).
[10] M. D. Radcliffe, M. L. Brostrom, K. A. Epstein, A. G. Rappaport, B. N. Thomas, R. F. Shao, and N. A. Clark, Liq. Cryst. **26**, 789 (1999).
[11] A. J. Leadbetter and E. K. Norris, Mol. Phys. **38**, 669 (1979).
[12] S. T. Lagerwall, P. Rudquist, and F. Giesselmann, Mol. Cryst. Liq. Cryst. **510**, 148 (2009).
[13] W. H. De Jeu and J. A. Poorter, Phys. Lett. A **61**, 114 (1977).
[14] A. Wulf, Phys. Rev. A **17**, 2077 (1978).
[15] M. Osipov and G. Pajak, Phys. Rev. E **85**, 021701 (2012).
[16] K. Saunders, Phys. Rev. E **77**, 061708 (2008); **80**, 011703 (2009).
[17] K. Saunders, D. Hernandez, S. Pearson, and J. Toner, Phys. Rev. Lett. **98**, 197801 (2007).
[18] M. V. Gorkunov, F. Giesselmann, J. P. F. Lagerwall, T. J. Sluckin, and M. A. Osipov, Phys. Rev. E **75**, 060701(R) (2007).
[19] M. V. Gorkunov, M. A. Osipov, J. P. F. Lagerwall, and F. Giesselmann, Phys. Rev. E **76**, 051706 (2007).
[20] H. G. Yoon, D. M. Agra-Kooijman, K. Ayub, R. P. Lemieux, and S. Kumar, Phys. Rev. Lett. **106**, 087801 (2011).
[21] C. C. Huang, S. T. Wang, X. F. Han, A. Cady, R. Pindak, W. Caliebe, K. Ema, K. Takekoshi, and H. Yao, Phys. Rev. E **69**, 041702 (2004).
[22] A. de Vries, Mol. Cryst. Liq. Cryst. **41**, 27 (1977).
[23] N. Kapernaum, D. M. Walba, E. Korblova, C. Zhu, C. Jones, Y. Shen, N. A. Clark, and F. Giesselmann, ChemPhysChem **10**, 890 (2009).
[24] Z. V. Kost-Smith, P. D. Beale, N. A. Clark, and M. A. Glaser, Phys. Rev. E **87**, 050502 (2013).
[25] M. D. Radcliffe, M. L. Brostrom, K. A. Epstein, A. G. Rappaport, B. N. Thomas, R. F. Shao, and N. A. Clark, Liq. Cryst. **26**, 789 (1999); L. Li, C. D. Jones, J. Magolan, and R. P. Lemieux, J. Mater. Chem. **17**, 2313 (2007).
[26] J. Naciri, C. Carboni, and A. K. George, Liq. Cryst. **30**, 219 (2003); N. A. Clark, T. Bellini, R.-F. Shao, D. Coleman, S. Bardon, D. R. Link, J. E. Maclennan, X.-H. Chenn, M. D. Wand, D. M. Walba, P. Rudquist, and S. T. Lagerwall, Appl. Phys. Lett. **80**, 4097 (2002).
[27] K. Goossens, K. Lava, P. Nockemann, K. Van Hecke, L. Van Meervelt, P. Pattison, K. Binnemans, and T. Cardinaels, Langmuir **25**, 5881 (2009).
[28] J. C. Roberts, N. Kapernaum, Q. Song, D. Nonnenmacher, K. Ayub, F. Giesselmann, and R. P. Lemieux, J. Am. Chem. Soc. **132**, 364 (2010).
[29] P. J. Collings, B. Ratna, and R. Shashidhar, Phys. Rev. E **67**, 021705 (2003); T. Murias, A. C. Ribeiro, D. Guillon, D. Shoosmith, and H. J. Coles, Liq. Cryst. **29**, 627 (2002).
[30] A. P. Hammersley, S. O. Svensson, M. Hanfland, A. N. Fitch, and D. Hausermann, High Pressure Res. **14**, 235 (1996).
[31] Y. Takanishi, Y. Ouchi, H. Takezoe, A. Fukuda, A. Mochizuki, and M. Nakatsuka, Mol. Cryst. Liq. Cryst. **199**, 111 (1991).
[32] H. S. Chang, S. Jaradat, H. F. Gleeson, I. Dierking, and M. A. Osipov, Phys. Rev. E **79**, 061706 (2009).
[33] A. J. Leadbetter and P. G. Wrighton, J. Phys. (Colloq.) **40**, C3-234 (1979).
[34] S. Diele, P. Brand, and H. Sackmann, Mol. Cryst. Liq. Cryst. **16**, 105 (1972).
[35] R. Bartolino, J. Doucet, and G. Durand, Ann. Phys. (Paris) **3**, 389 (1978).
[36] Q. Song, D. Nonnenmacher, F. Giesselmann, and R. P. Lemieux, Chem. Commun. **47**, 4781 (2011).
[37] P. Davidson, D. Petermann, and A. M. Levelut, J. Phys. II **5**, 113 (1995).
[38] N. Hayashi, T. Kato, A. Fukuda, J. K. Vij, Y. P. Panarin, J. Naciri, R. Shashidhar, S. Kawada, and S. Kondoh, Phys. Rev. E **71**, 041705 (2005).
[39] A. Sanchez-Castillo, M. A. Osipov, S. Jagiella, Z. H. Nguyen, M. Kaspar, V. Hamplova, J. Maclennan, and F. Giesselmann, Phys. Rev. E **85**, 061703 (2012).
[40] J. P. F. Lagerwall, F. Giesselmann, and M. D. Radcliffe, Phys. Rev. E **66**, 031703 (2002).
[41] N. Clark, T. Bellini, R. Shao, D. Coleman, S. Bardon, D. R. Link, J. E. Maclennan, X.-H. Chen, M. D. Wand, P. Rudquist, and S. T. Lagerwall, Appl. Phys. Lett. **80**, 4097 (2002).
[42] J. V. Selinger, P. J. Collings, and R. Shashidhar, Phys. Rev. E **64**, 061705 (2001).
[43] J. Prost, Adv. Phys. **33**, 1 (1984), and references therein.
[44] J. Wang and T. C. Lubensky, Phys. Rev. A **29**, 2210 (1984); T. C. Lubensky, S. Ramaswamy, and J. Toner, *ibid.* **38**, 4284 (1988).
[45] P. Patel, S. Kumar, and P. Ukleja, Liq. Cryst. **16**, 351 (1994).
[46] P. Patel, S. S. Keast, M. E. Neubert, and S. Kumar, Phys. Rev. Lett. **69**, 301 (1992).